Improved Determination of the Mobility and Built-In Voltage in Asymmetric Single-Carrier Devices

G.A.H. Wetzelaer*

Max Planck Institute for Polymer Research, Ackermannweg 10, 55128 Mainz, Germany

(Received 1 August 2019; revised manuscript received 4 October 2019; accepted 6 March 2020; published 27 March 2020)

The steady-state charge-carrier mobility in semiconductors can be extracted from the space-charge-limited current in single-carrier devices. However, in many cases, a built-in voltage is present, which should be known accurately to obtain the correct mobility. Here, it is demonstrated that band bending at the injecting electrode has important consequences for the built-in voltage and the analytical description of the current-voltage characteristics. It is shown that the built-in voltage can be accurately determined from the slope of the current-voltage characteristics on a semilogarithmic scale. Knowing the effect of band bending on the injected current, a simple analytical equation for the drift-diffusion space-charge-limited current above the built-in voltage is derived, which allows for improved determination of the charge-carrier mobility from experimental data.

DOI: 10.1103/PhysRevApplied.13.034069

A widely used method to determine the charge-carrier mobility in semiconductors and organic semiconductors, in particular, is the measurement of space-charge-limited currents [1,2]. To do so, single-carrier devices are prepared, in which, depending on the work functions of the electrodes, either the electron or hole current through the semiconductor is measured as a function of the applied voltage. In the case of asymmetric electrode work functions, a built-in voltage exists [3,4], giving rise to a built-in electric field. For voltages below the built-in voltage, the current is dominated by diffusion of charge carriers, whereas above the built-in voltage the current is dominated by drift [5]. In the case of an Ohmic injecting electrode on an undoped semiconductor without traps, a space-charge-limited current is obtained, as described by the drift-only approximation given by the Mott-Gurney square law [6]:

$$J_{\mathrm{drift}} = \frac{9}{8}\varepsilon\mu\frac{(V-V_{\mathrm{BI}})^2}{L^3}, \tag{1}$$

where J_{drift} is the current density, V is the voltage, V_{BI} is the built-in voltage, ε is the permittivity, μ is the charge-carrier mobility, and L is the layer thickness. Equation (1) is valid only for $V > V_{\mathrm{BI}}$ and knowledge of the built-in voltage is essential when fitting this equation to experimental data to obtain the mobility.

*wetzelaer@mpip-mainz.mpg.de

The built-in voltage has previously been obtained by electroabsorption measurements [3], photovoltaic measurements [4], and capacitance-voltage measurements [7]. However, these methods do not always give an accurate estimate of the built-in voltage [8]. Alternatively, built-in voltages can be estimated by fitting J-V characteristics with drift-diffusion simulations [5,9,10] or can be obtained by means of charge-extraction measurements [11]. Recently, a method was proposed to extract the built-in voltage directly from the ratio of the forward and reverse currents of a single-carrier device, based on drift-diffusion simulations [12]. While this method has potential, care should be taken to account for band bending at the injecting contact, which modifies the built-in voltage. Here, it is demonstrated that band bending has crucial implications for the built-in voltage and, as a result, characterization of the mobility with Eq. (1). By accounting for band bending, it is demonstrated that a near-perfect agreement between numerical simulations and analytical equations for the drift-diffusion current is obtained. Based on this result, a method is proposed to extract the built-in voltage directly from current-voltage characteristics. Having established the importance of band bending on the diffusion current and the built-in voltage, a simple analytical expression for the space-charge-limited current above the built-in voltage is derived, containing both drift and diffusion. This equation allows for direct determination of the mobility from experimental current density-voltage characteristics, leading to an improvement over the widely used Mott-Gurney law.

In Fig. 1, a schematic depiction of the band diagram of an electron-only device is given. The barrier at the injecting electrode (cathode) is zero, leading to sharp band

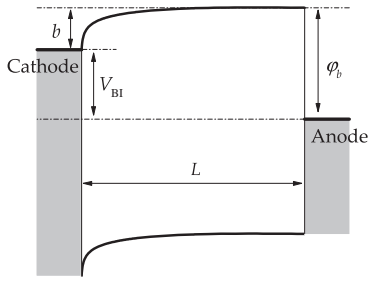

FIG. 1. Schematic energy-band diagram for a semiconductor of thickness L between an Ohmic injecting cathode and an electron-extracting anode with barrier φ_b, under an applied voltage equal to the built-in voltage. Built-in voltage is defined by the Fermi-level difference between anode and cathode, given by $V_{BI} = \varphi_b - b$, where b the band-bending parameter at the Ohmic cathode. Reprinted with permission from G. A. H. Wetzelaer, AIP Advances, 8, 035320 (2018). Copyright 2018, AIP Publishing.

bending in the vicinity of the cathode caused by the accumulation of diffused charge carriers. The amount of band bending is quantified by parameter b. The barrier φ_b at the extracting electrode (anode) is nonzero and band bending near this electrode is therefore absent. As a result, a built-in voltage is present, which is given by $V_{BI} = \varphi_b - b$, resulting in a quasi-flat-band situation for $V = V_{BI}$, as shown in Fig. 1. This demonstrates that band bending at the injecting contact has important implications for the internal field in the device. Neglecting band bending would lead to an overestimation of the internal electric field and V_{BI}. In addition, disregarding the band-bending parameter results in severe overestimation of the diffusion current, as demonstrated in the following.

As derived previously [5], the diffusion-dominated current density in an organic metal-insulator-metal device is given by

$$J_{\text{diff}} = \frac{q\mu N_C(\varphi_b - b - V)\left[\exp\left(\frac{qV}{kT}\right) - 1\right]}{L\left[\exp\left(\frac{q\varphi_b}{kT}\right) - \exp\left(\frac{q(V+b)}{kT}\right)\right]}, \qquad (2)$$

where q is the elementary charge, N_C is the density of states, φ_b is the barrier at the extracting contact, k is the Boltzmann constant, T is the temperature, and b is the band-bending parameter given by [5]

$$b = \frac{kT}{q}\ln\left[\frac{q^2 N_C L^2}{2\exp(2)kT\varepsilon}\right]. \qquad (3)$$

The inclusion of a band-bending parameter, b, is of critical importance not only for the correct description of the built-in voltage, but even more so for the correct magnitude of the current, especially in forward bias. This is displayed in Fig. 2(a), where the drift [Eq. (1)] and diffusion [Eq. (2)] contributions to the current are compared with numerical drift-diffusion simulations [14], which is an approach that is also followed in Ref. [12]. The same parameters are used: $N_C = 10^{25}$ m^{-3}, $\mu = 10^{-8}$ m^2/Vs, $T = 295$ K, and $L = 100$ nm. For boundary conditions in the numerical simulations, the barrier at the injecting electrode is set to zero, while varying the barrier φ_b at the extracting electrode. These parameters lead to a band-bending parameter of $b = 0.19$ V [Eq. (3)]. Notably, for organic semiconductors, more realistic values of N_C of approximately 10^{27} m^{-3} (corresponding to a site spacing of 1 nm) lead to a parameter b of approximately 0.3 V, which has a larger effect on the built-in voltage. As demonstrated in Fig. 2(a), agreement between the analytical and numerical description is clearly superior to that obtained when neglecting band bending at the injecting contact (red lines). In this case, the built-in voltage is overestimated, leading to a disagreement between the Mott-Gurney law and the numerical simulations. In addition, the diffusion current is greatly overestimated due to the nonphysical boundary conditions at the injecting electrode.

When including band bending, summing of the drift and diffusion currents, as described separately by Eqs. (1) and (2), results in a near-perfect agreement with the numerical simulations, as shown in Fig. 2(b). This agreement also holds when varying the input parameters, as shown in

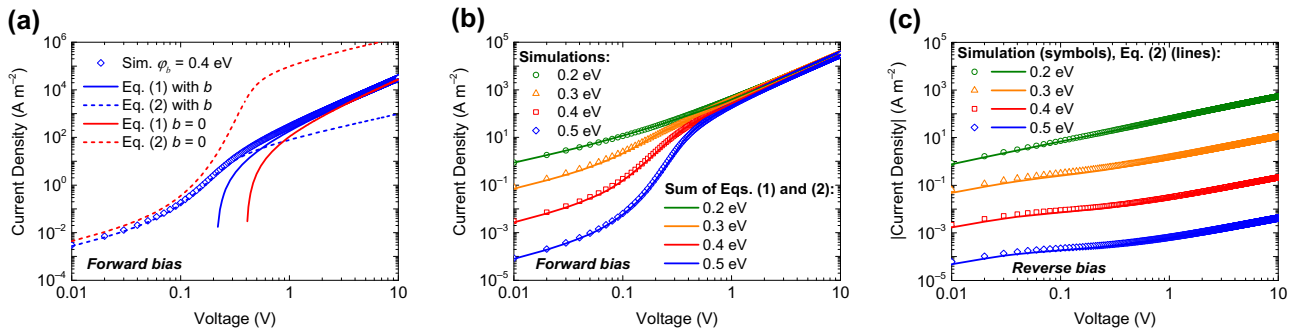

FIG. 2. Current density as a function of voltage. (a) Numerical simulations (symbols) of the current in forward bias for a barrier φ_b of 0.4 eV. Solid and dashed lines are drift and diffusion currents calculated with Eqs. (1) and (2), respectively, for the case with band bending according to Eq. (3) and for $b = 0$. (b) Numerical simulations (symbols) for different barriers φ_b, compared with analytical results calculated by summing Eqs. (1) and (2). (c) Same as (b) for reverse bias; the current has negative values.

the Supplemental Material [15]. Also, the injection-limited reverse-bias current is now correctly reproduced by Eq. (2), as displayed in Fig. 2(c). Notably, the Mott-Gurney law [Eq. (1)] is not applicable in reverse bias, since the injecting contact is non-Ohmic, preventing the buildup of space charge. The accurate description provided by Eqs. (1) and (2) in forward and reverse bias is due to a combination of the correct definition of both the built-in voltage and the boundary conditions at the injecting electrode.

It is clear that the analytical current equations only reproduce the numerical simulations when band bending is taken into account. Using the sum of the drift and diffusion current, a correct analytical description is obtained, which can be used to fit experimental data without using numerical modeling. This approach can even be applied to disordered semiconductors [13]. In the simplest case of using only Eq. (1) to fit experimental data, it is still important to use the correct built-in voltage, as shown below for the case of an organic-semiconductor device. When disregarding band bending, the built-in voltage will be overestimated, by typically 0.3 V, which leads to an overcorrection of the experimental J-V characteristics and, in turn, results in an overestimation of the charge-carrier mobility.

To obtain the built-in voltage and mobility from experimental data, the drift-diffusion current [sum of Eqs. (1) and (2)] can be fitted to the measured J-V characteristics. The built-in voltage will shift the calculated J-V characteristics horizontally along the voltage axis, while the mobility will shift the J-V characteristics vertically, so that both parameters can be obtained independently. Another, somewhat empirical, method to obtain the built-in voltage independent of the mobility has been described previously [16]. Here, the built-in voltage is obtained from the transition from the exponential diffusion regime to the quadratic drift regime, which can be observed on a semilogarithmic J-V plot, as shown in Fig. 3(a). The same simulation parameters are used as those in Fig. 2. To show the validity and to improve the precision of this method, the slopes of numerically simulated J-V characteristics, $d\ln(J)/dV$, are depicted in Fig. 3(b). At low voltages ($V < V_{\mathrm{BI}}$) in the diffusion-dominated regime, the slope of the exponential J-V characteristics approaches $q/(kT)$. With increasing voltage, the slope reduces, marking the transition to the drift-dominated regime. The transition point is characterized by the voltage at which the slope reaches a value of $q/(2kT)$, which is half of the slope in the diffusion-dominated exponential J-V region. Indeed, the derivative $d\ln(J)/dV$ of the analytical diffusion current [Eq. (2)] in the limit of $V \to V_{\mathrm{BI}}$ equals $q/(2kT)$, which confirms that the transition in slope corresponds to the built-in voltage. As shown in Fig. 3(b), the extracted built-in voltages from the derivatives of the numerical simulations are also very close to $V_{\mathrm{BI}} = \varphi_b - b$, demonstrating that the built-in voltage can be reliably extracted from the slope of the J-V characteristics. It should be noted that this method to obtain V_{BI} is independent of the parameters used, such as the density of states, mobility, temperature, layer thickness, or the relative permittivity.

For voltages larger than the built-in voltage, a simplified expression for the drift-diffusion current can be derived. First, Eq. (3) is substituted into Eq. (2), followed by expressing Eq. (2) in terms of V_{BI}. By summing Eqs. (1) and (2), the current density for $V > V_{\mathrm{BI}}$ in an asymmetric single-carrier device ($V_{\mathrm{BI}} \gg kT/q$), including both drift and diffusion, is then described by

$$J = \left[\frac{2\exp(2)}{1-\exp\left(\frac{q(V_{\mathrm{BI}}-V)}{kT}\right)}\frac{kT}{q} + \frac{9}{8}(V - V_{\mathrm{BI}})\right]\varepsilon\mu\frac{(V-V_{\mathrm{BI}})}{L^3}, \tag{4}$$

which is compared to numerical simulations in Fig. 3(a) and can be further reduced for $V - V_{\mathrm{BI}} \gg kT/q$ to the

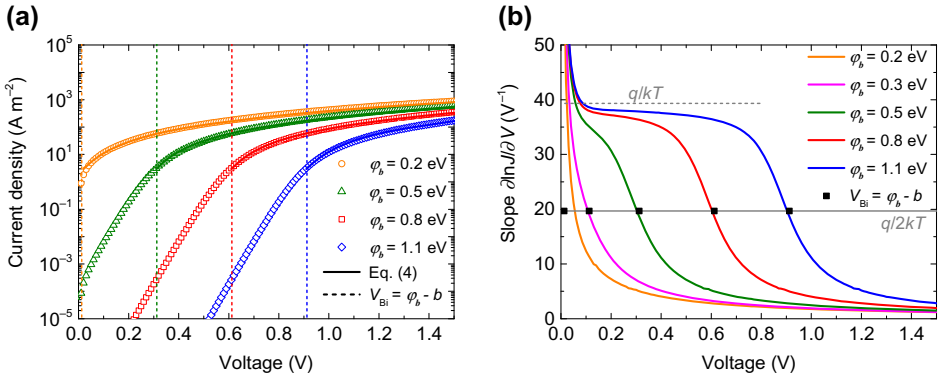

FIG. 3. (a) Numerical simulations (symbols) of current density as a function of voltage on a semilogarithmic scale for different barriers φ_b at the extracting electrode. Vertical dashed lines mark the built-in voltage, according to $V_{\mathrm{BI}} = \varphi_b - b$, corresponding to the transition from diffusion to drift. Solid lines are analytical calculations according to Eq. (4). (b) Corresponding derivative of $\ln(J)$ versus V. Voltage at which the slope reaches a value of $q/2kT$ coincides with the built-in voltage defined by $V_{\mathrm{BI}} = \varphi_b - b$.

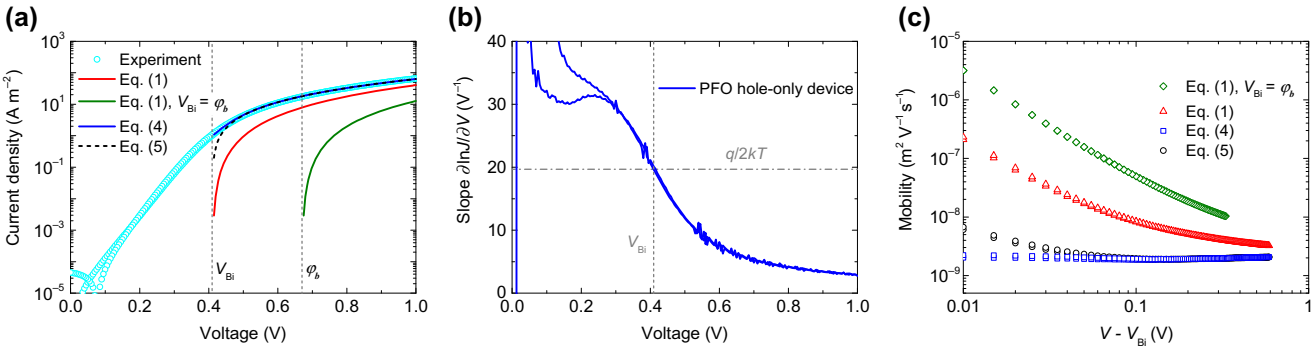

FIG. 4. (a) Experimental J-V characteristic of a PFO hole-only device (symbols) and calculated J-V characteristics above V_{BI} (vertical dashed lines), with the green line calculated for $V_{BI} = \varphi_b$, neglecting band bending. (b) Derivative of the experimental J-V characteristic, indicating the built-in voltage (vertical dashed line). (c) Hole mobility extracted with different equations.

relatively simple expression

$$J = \left[2\exp(2)\frac{kT}{q} + \frac{9}{8}(V - V_{BI})\right]\varepsilon\mu\frac{(V - V_{BI})}{L^3}. \quad (5)$$

Notably, Eq. (5) contains only the mobility and built-in voltage as unknown parameters. With the built-in voltage determined from the transition from the exponential diffusion current to the quadratic drift current, Eqs. (4) or (5) can be used to extract the charge-carrier mobility from experimental J-V characteristics as an improved alternative to the Mott-Gurney law [Eq. (1)].

As an example of applying these methods to experimental data, a hole-only device of the conjugated polymer poly(9,9-dioctylfluorene) (PFO) is considered, in which an 80 nm PFO layer is situated between a hole-extracting poly(3,4-ethylenedioxythiophene):polystyrene sulfonate (PEDOT:PSS) bottom electrode and a hole-injecting MoO_3(10 nm)/Al(100 nm) top electrode. Here, PEDOT:PSS was spin coated from a water-based dispersion on top of an indium tin oxide covered glass substrate, while the MoO_3/Al top electrode was thermally evaporated under high vacuum. The PFO layer was spin coated from a toluene solution, without further annealing of the film.

Due to the difference between the work function of the PEDOT:PSS bottom electrode (5.1 eV) and the ionization energy of PFO (5.8 eV), a barrier at the extracting electrode φ_b of approximately 0.7 eV is expected. This energetic picture can be verified when extracting the built-in voltage from the slope of the experimental J-V characteristic on a semilogarithmic plot [Fig. 4(a)], as displayed in Fig. 4(b). The built-in voltage, corresponding to the voltage at which the slope has a value of $q/2kT$, amounts to 0.41 V.

With V_{BI} known, the mobility can be obtained directly from experimental data with Eq. (4) or its simplified version, Eq. (5). With Eqs. (4) and (5), the mobility is obtained correctly, even at voltages very close to V_{BI}, as displayed in Fig. 4(c). This can be seen from the negligible overestimation of the mobility at low voltage, which is due to the inclusion of diffusion in Eqs. (4) and (5). The obtained mobility is also in close agreement with transient electroluminescence measurements on similarly prepared films [17]. As expected, when estimating the mobility with the drift-only approximation [Eq. (1) (Mott-Gurney law)], the mobility can only be obtained at higher applied voltage, where diffusion is negligible. At low voltages, the apparent mobility is overestimated significantly, which is caused by neglecting the diffusion contribution to the current. The mismatch at low voltages becomes more severe when band bending is also neglected. With b calculated to be 0.26 V [Eq. (3)] and $V_{BI} = 0.41$ V, φ_b amounts to 0.67 V, which is in agreement with the expected barrier of 0.7 eV. Taking the built-in voltage to be equal to φ_b leads to a severe overestimation of the mobility at low voltages. As a result, it is demonstrated that Eqs. (4) and (5), in combination with the proposed method to obtain V_{BI}, constitute an improved method to obtain low-voltage mobility in single-carrier devices.

With the mobility known, the analytical calculations of the current density are compared with experimental data. These simple expressions for the drift-diffusion current, Eqs. (4) and (5), are in excellent agreement with experiment, using a mobility of 2×10^{-9} m^2/Vs. Equation (1) still works reasonably well when using the correct built-in voltage, if sufficient voltage is applied for the current to be fully drift dominated. When the effect of band bending on the built-in voltage is neglected ($V_{BI} = \varphi_b$), the calculated current severely underestimates the experimental data.

In conclusion, it is shown that including band bending is critical for describing both the built-in voltage and the drift and diffusion currents in asymmetric single-carrier devices. It is demonstrated that the built-in voltage can be accurately obtained from the transition between the exponential diffusion-dominated regime and the quadratic drift regime. Based on these results, a simple

expression for the drift-diffusion current above the built-in voltage is derived and can be used to extract the mobility directly from experimental data. The derived equation is an improvement over the widely used drift-only approximation of the space-charge-limited current, namely, the Mott-Gurney square law.

[1] M. Stolka and M. A. Abkowitz, Trap-free charge transport in polymers, with tunable mobilities, Synth. Met. **54**, 417 (1993).

[2] J. C. Blakesley, F. A. Castro, W. Kylberg, G. F. A. Dibb, C. Arantes, R. Valaski, M. Cremona, J. S. Kim, and J.-S. Kim, Towards reliable charge-mobility benchmark measurementsfor organic semiconductors, Org. Electron. **15**, 1263 (2014).

[3] I. H. Campbell, T. W. Hagler, D. L. Smith, and J. P. Ferraris, Direct Measurement of Conjugated Polymer Electronic Excitation Energies Using Metal/Polymer/Metal Structures, Phys. Rev. Lett. **76**, 1900 (1996).

[4] G. G. Malliaras, J. R. Salem, P. J. Brock, and J. C. Scott, Photovoltaic measurement of the built-in potential in organic light emitting diodes and photodiodes, J. Appl. Phys. **84**, 1583 (1998).

[5] P. de Bruyn, A. H. P. van Rest, G. A. H. Wetzelaer, D. M. de Leeuw, and P. W. M. Blom, Diffusion-Limited Current in Organic Metal-Insulator-Metal Diodes, Phys. Rev. Lett. **111**, 186801 (2013).

[6] N. F. Mott and R. W. Gurney, *Electronic Processes in Ionic Crystals* (Oxford University Press, London, 1940).

[7] S. L. M. van Mensfoort and R. Coehoorn, Determination of Injection Barriers in Organic Semiconductor Devices From Capacitance Measurements, Phys. Rev. Lett. **100**, 086802 (2008).

[8] R. J. de Vries, S. L. M. van Mensfoort, R. A. J. Janssen, and R. Coehoorn, Relation between the built-in voltage in organic light-emitting diodes and the zero-field voltage as measured by electroabsorption, Phys. Rev. B **81**, 125203 (2010).

[9] J. A. Röhr, X. Shi, S. A. Haque, T. Kirchartz, and J. Nelson, Charge Transport in Spiro-OMeTAD Investigated Through Space-Charge-Limited Current Measurements, Phys. Rev. Appl. **9**, 044017 (2018).

[10] X. Shi, V. Nádaždy, A. Perevedentsev, J. M. Frost, X. Wang, E. von Hauff, R. C. I MacKenzie, and J. Nelson, Relating Chain Conformation to the Density of States and Charge Transport in Conjugated Polymers: The Role of the β-Phase in Poly(9,9-Dioctylfluorene), Phys. Rev. X **9**, 021038 (2019).

[11] S. Dahlström, O. J. Sandberg, M. Nyman, and R. Österbacka, Determination of Charge-Carrier Mobility and Built-In Potential in Thin-Film Organic M-I-M Diodes From Extraction-Current Transients, Phys. Rev. Appl. **10**, 054019 (2018).

[12] J. A. Röhr, Direct Determination of Built-in Voltages in Asymmetric Single-Carrier Devices, Phys. Rev. Appl. **11**, 054079 (2019).

[13] G. A. H. Wetzelaer, Analytical description of the current-voltage relationship in organic-semiconductor diodes, AIP Adv. **8**, 035320 (2018).

[14] L. J. A. Koster, E. C. P. Smits, V. D. Mihailetchi, and P. W. M. Blom, Device model for the operation of polymer/fullerene bulk heterojunction solar cells, Phys. Rev. B **72**, 085205 (2005).

[15] See the Supplemental Material at http://link.aps.org/supplemental/10.1103/PhysRevApplied.13.034069 for current-voltage characteristics with different parameters.

[16] V. D. Mihailetchi, P. W. M. Blom, J. C. Hummelen, and M. T. Rispens, Cathode dependence of the open-circuit voltage of polymer:Fullerene bulk heterojunction solar cells, J. Appl. Phys. **94**, 6849 (2003).

[17] H. T. Nicolai, G. A. H. Wetzelaer, M. Kuik, A. J. Kronemeijer, B. de Boer, and P. W. M. Blom, Space-charge-limited hole current in poly(9,9-dioctylfluorene) diodes, Appl. Phys. Lett. **96**, 172107 (2010).